Performance Analysis of Data Packet Discarding in ATM Networks *

Yonghwan Kim *San-qi Li*
Department of Electrical and Computer Engineering
University of Texas at Austin
Austin, Texas 78712
{kyh,sanqi}@globe.ece.utexas.edu

Abstract

Data performance in ATM networks should be measured on packet level instead on cell level, since one or more cell losses within each packet is equivalent to the loss of the entire packet. Two control schemes, packet tail discarding (PTD) and early packet discarding (EPD), were proposed to improve the data performance. This paper develops a stochastic modeling technique for performance evaluation of PTD and EPD scheme at a single node. In numerical study, we explore the effects of buffer capacity, control threshold, packet size, source access rate, window size, underlying high-priority real-time traffic and loading factor on data performance and discuss their design trade-off. Our study shows that the system can be entirely shut down in overload period if no packet discarding control scheme is implemented. Further, unless with sufficiently large buffer capacity, EPD always outperforms PTD significantly under most conditions. Especially under overload condition, EPD can always achieve about 100% goodput and 0% badput whereas the performance of PTD deteriorates rapidly. Among all the factors, the packet size has dominant impact on EPD performance. In the design of EPD, there is an optimal selection of the queue control threshold to achieve the maximum goodput.

*The research reported here was supported by NSF under grant NCR-9314387, Southwestern Bell, and by Texas Advanced Research Program under grant TARP-33. This paper will be partly presented at *15th International Teletraffic Congress*, Washington D. C., June, 1997.

1 Introduction

Most existing performance analyses of ATM networks are based on cell level. Namely, the service quality is measured by cell loss rate and cell delay variation; the link transmission efficiency is described by cell-based utilization. Such measurement are not appropriate to many of the data services. Before its transmission in ATM networks, a data message is first disassembled into packets, each of which is further disassembled into cells. Since no flow control is designed to recover individual lost cells within each packet in ATM networks, a data packet experiencing one or more cell losses is regarded as a failed packet. Although a failed packet means a whole packet loss to the end-user, it is further classified as a *corrupted* or *lost* packet at the local node. A data packet is corrupted if some of its cells are still transmitted through the local node. A data packet is lost at the local node if none of its cells are transmitted. It is obvious that data performance should be measured on packet level, i.e., counting for packet-based throughput and loss probability. There are two types of packet throughput: goodput and badput. The goodput is the throughput of successfully transmitted packets. The badput is the throughput of corrupted packets, which provides a measure of wasted network resources.

Packets get lost in two ways: they are corrupted due to transmission error, or the network is congested. With the improvement of optical technology, loss due to transmission error becomes negligible so a packet loss is most likely due to network congestion [1]. Two data packet discarding schemes were proposed to improve the data performance at each switching node [2, 3]: packet tail discarding (PTD) and early packet discarding (EPD). PTD was called *selective cell discarding* in [2] and *partial packet discard* in [3]. The PTD scheme is designed to block the tail portion of each arriving packet when the buffer is full. Since the occurrence of a single cell loss will fail the entire packet transmission, it is unnecessary to send the remaining cells of the packet and so the saved buffer capacity and link bandwidth improves the transmission of other packets. The EPD scheme is designed to block the entire cell stream of each newly arriving packet whenever the buffer exceeds a certain threshold. Since less number of corrupted packets are transmitted by the EPD scheme, the data performance is further improved. Another congestion control called random early detection (RED) is proposed in [4], which is also based on buffer threshold. The threshold in RED would be lower than EPD threshold and is to control the average queue size. In [3], the implementation of EPD in conjunction with RED is suggested.

So far there have been no stochastic analyses available for performance evaluation of the EPD scheme. The pioneer work on this subject was done by simulation in [3], where the performance of PTD and EPD on 10 TCP connections was evaluated. In [5], *Turner* studied the behavior of PTD scheme and provides a worst-case deterministic analysis of EPD scheme. Recently in [6], *Kamal* analyzed the packet blocking probability and the average delay of successful packets for the PTD scheme. For the earlier work in this regime, *Bhargava* and *Hluchyj* also presented an analytical method to estimate the bound of frame loss probabilityby fluid-flow approximation [7]. Compared to these works, our paper provides a general solution technique for the evaluation of packet-level throughput, goodput and badput, and packet loss probability for both EPD and PTD schemes.

In this paper, we develop a generic stochastic modeling technique for the performance evaluation of PTD and EPD control schemes based on finite Quasi-Birth Death (QBD) modeling. As one will see, the formulation of various performance measurements leads to systems of linear equations of the type $\mathbf{xG} = \mathbf{a}$, where $\mathbf{G}$ is a matrix with block tri-diagonal structure. The numerical solution $\mathbf{x}$ is then derived by the Generalized Folding Algorithm (GFA) [8]. In numerical study, we will systematically examine the effects of buffer capacity, control threshold, packet size, source access rate, window size, underlying priority real-time traffic and loading factor on the performance of packet goodput, badput and loss probability.

The paper is organized as follows. Section 2 provides packet-level performance measurements and the background materials on transient QBD modeling. Section 3 shows the formulation of packet goodput,

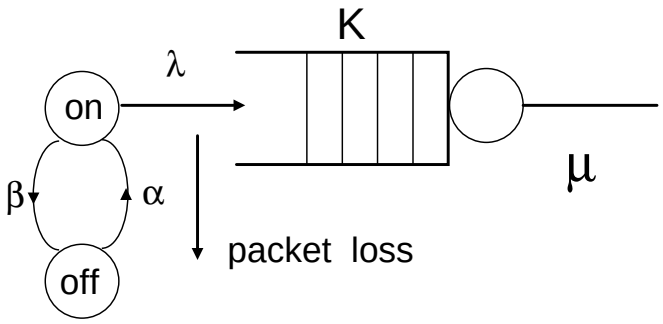

Figure 1: Modeling of a packet transmission.

badput and loss probability for a single ON/OFF source on a finite-buffer queueing system with PTD and EPD. The analysis is then extended to multiple ON/OFF sources in Section 4. Section 5 shows the performance trade off in the PTD and EPD design. Section 6 is the conclusion.

Throughout the paper, we use the following rules for the notations. Matrices are represented by bold face capital letters such as $\mathbf{A}$, $\mathbf{B}$, and $\mathbf{Q}$; Vectors are by bold face small letters such as $\mathbf{a}$, $\mathbf{b}$ and $\boldsymbol{\alpha}$; and numbers are by italic capital letters such as K, M, and N. We further use $\mathbf{I}$ for identity matrix and $\mathbf{e}$ for unit column vector with appropriate dimension.

2 Performance Measurement and QBD Modeling

A data packet stream can be described by an ON/OFF model, where each ON period represents the generation of one packet at a constant rate and each OFF period is the inactive period between adjacent packets. In stochastic modeling, each ON/OFF source is characterized by a two-state Markov chain. The sojourn time in ON and OFF states are exponentially distributed at rate β and α, respectively. While in ON state, cells are generated at the Poisson rate λ. Hence, each packet generates cells at rate λ for the average duration of β^{-1}, providing the average packet size $\lambda\beta^{-1}$ in cell units.

Fig. 1 shows a finite buffer system with a single source and a single server. A packet is successfully transmitted if and only if none of its arriving cells are blocked by the queue. A packet is corrupted if its cells are only partially delivered. Given a normalized loading factor ρ, the cell level performance is typically measured by the average cell loss rate L_c. The total throughput is then given by $(1-L_c)\rho$. For packet level performance, we need to divide the throughput into goodput ρ_g and badput ρ_b with $\rho_g+\rho_b = (1-L_c)\rho$. The goodput is defined for the transmitted cells of successful packets; the badput is defined for the transmitted cells of corrupted packets. We further need to evaluate the probability for a packet to succeed, denoted by P_g. For deterministic packet size, one can directly relate P_g to ρ_g once the packet size is given. For random packet size, however, there is no such a direct relationship between ρ_g and P_g. Since a shorter packet is more likely to succeed than a longer one; the average size of successful packets is actually less than the average size of total generated packets. As one will see, the evaluation of ρ_g and ρ_b requires the computation of the average successful packet size. The packet level data performance is therefore measured by L_c, ρ_b, ρ_g and P_g. In our analysis, since $\rho_g + \rho_b = (1 - L_c)\rho$, we only need to display the results of (ρ_g, ρ_b, P_g) with respect to different packet discarding schemes.

Assume that the queueing system is modeled by an exponential server at rate μ and a finite buffer capacity of K cells with FCFS scheduling. The aggregate cell arrival process is superimposed by independent ON/OFF sources. For cell-level performance analysis, such a system is typically described by an MMPP/M/1/K queueing model which has the structure of finite QBD. For packet-level performance

analysis, we need to expand each two-state Markov chain source to a three-state Markov chain in order to distinguish successful packets from corrupted/lost packets while in ON state. The basic QBD structure remains unchanged by such expansion. Yet, the packet-level analysis will require both steady-state and transient-state QBD analyses.

Before the detailed modeling, let us first describe some basic results in QBD analysis. The generator matrix $\mathbf{G}$ of a finite QBD process has the following block-tridiagonal structure:

$$\mathbf{G} = \begin{bmatrix} \mathbf{A}_0 & \mathbf{U} & & & & \\ \mathbf{D} & \mathbf{A} & \mathbf{U} & & & \\ & \ddots & \ddots & \ddots & & \\ & & \mathbf{D} & \mathbf{A} & \mathbf{U} & \\ & & & \mathbf{D} & \mathbf{A}_1 & \end{bmatrix}, \tag{1}$$

where each block is a submatrix of dimension N and there are totally $K+1$ rows of blocks in $\mathbf{G}$. In the two-dimensional QBD state definition, N is the dimension of phases and $K+1$ is the dimension of levels. For a steady-state QBD process, let $\boldsymbol{\pi} = [\boldsymbol{\pi_0}\ \boldsymbol{\pi_1}\ \cdots\ \boldsymbol{\pi_K}]$ be the steady-state probability solution vector, where $\boldsymbol{\pi_i}$ is a sub-row-vector for the steady-state probability on level i. $\boldsymbol{\pi}$ is the unique solution of

$$\boldsymbol{\pi}\mathbf{G} = \mathbf{0} \tag{2}$$

with normalizing equation $\boldsymbol{\pi}\mathbf{e} = 1$. It can be numerically solved by the Folding algorithm [9], which also allows level-dependent transitions in the QBD modeling for control analysis.

For a transient-state QBD process, its tridiagonal generator matrix $\mathbf{G}_1$ is defined on a transient state space $\boldsymbol{\Omega}_1$. The transient process terminates in an absorbing state subspace $\boldsymbol{\Omega}_a$, described by a Markovian state transition matrix $\mathbf{Q}_{1a}$ from $\boldsymbol{\Omega}_1$ to $\boldsymbol{\Omega}_a$. Conditioned on a starting state $X_i \in \boldsymbol{\Omega}_1$, the probability for the transient process to terminate in state $X_j \in \boldsymbol{\Omega}_a$ is denoted by b_{ij}. From the general Markov chain matrix theory [10], one can obtain the conditional probability matrix $\mathbf{B} = [b_{ij}]$ from

$$\mathbf{G}_1\mathbf{B} = -\mathbf{Q}_{1a} \tag{3}$$

which is numerically solvable by the generalized Folding algorithm [8]. Further, if we know the probability vector $\boldsymbol{\alpha}_{in}$ for the transient process to start at different states in $\boldsymbol{\Omega}_1$, the jth element of the vector $\boldsymbol{\alpha}_{in}\mathbf{B}$ gives the unconditional probability vector for the transient process to terminate in $X_j \in \boldsymbol{\Omega}_a$.

Note that the (i,j)th element of $-\mathbf{G}_1^{-1}$ gives the average sojourn time in the transient state $X_j \in \boldsymbol{\Omega}_1$ conditioned on starting state $X_i \in \boldsymbol{\Omega}_1$. We are also interested in the average sojourn time in each state of $\boldsymbol{\Omega}_1$ given that the transient chain started in $X_i \in \boldsymbol{\Omega}_1$ and conditioned on its absorption in a particular state $X_j \in \boldsymbol{\Omega}_a$. Denote by b_{ij} the probability for the transient process to be absorbed in state X_j given the starting state X_i as defined above. Introducing a diagonal matrix $\mathbf{D}_j = \text{diag}\{b_{ij}, \forall i\}$, then the average sojourn time matrix conditioned on the absorption in X_j will be given by [10]

$$\overline{\mathbf{T}}_j = -\mathbf{D}_j^{-1}\mathbf{G}_1^{-1}\mathbf{D}_j, \tag{4}$$

which is equivalent to computing $\overline{\mathbf{T}}_j = \mathbf{D}_j^{-1}\mathbf{X}$, where $\mathbf{X}$ may be obtained from $\mathbf{G}_1\mathbf{X} = -\mathbf{D}_j$ by the generalized Folding algorithm.

3 Modeling with a Single ON/OFF Source

This section develops the basic technique for the evaluation of $(L_c, \rho_g, \rho_b, P_g)$ using a single ON/OFF source, with respect to different packet discarding schemes.

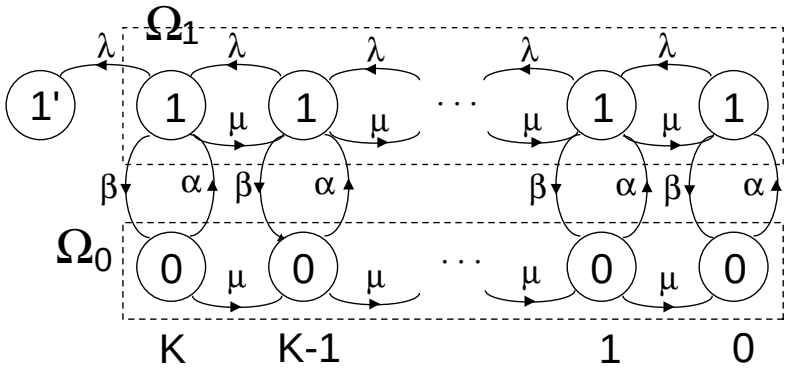

Figure 2: Modeling of no packet discarding with a single source.

3.1 Without Packet Discarding

The queueing system with a single ON/OFF source is simply modeled by a regular QBD process with its state space defined by $\mathbf{\Omega} = \{(i,j)|i = 0,1;\ j = 0,1,...,K\}$. The steady state solution vector $\boldsymbol{\pi}$ can then be derived by (2). The cell loss probability L_c is expressed by

$$L_c = \frac{\lambda}{\overline{\gamma}}\pi_{1K}\,, \tag{5}$$

where $\overline{\gamma}$ is the average arrival rate equal to $\frac{\alpha\lambda}{\alpha+\beta}$. The link utilization is given by $\rho(1-L_c)$ where $\rho = \frac{\overline{\gamma}}{\mu}$ is the normalized loading factor.

To characterize each individual packet transmission, we need to divide $\mathbf{\Omega}$ into two disjoint sets: $\mathbf{\Omega_1} = \{(1,j)|j = 0,1,...,K\}$ for source in ON state and $\mathbf{\Omega_0} = \{(0,j)|j = 0,1,...,K\}$ for source in OFF state, each of which is associated with a transient process. As shown in Fig. 2, whenever the source turns on to start sending a packet, the QBD process takes a phase-up transition from $\mathbf{\Omega_0}$ to $\mathbf{\Omega_1}$ at rate α. Similarly, whenever the source turns off to terminate packet generation, the QBD process takes a phase-down transition from $\mathbf{\Omega_1}$ to $\mathbf{\Omega_0}$ at rate β. Cells of each packet are generated at rate λ while in $\mathbf{\Omega_1}$. Hence, a packet transmission is successful if no cell arrivals are blocked during its entire generation time. Since the cells can only be blocked when the buffer is full, each blocked cell in a packet is characterized by a cell arrival transition at rate λ when the buffer is at the level K in $\mathbf{\Omega_1}$, as shown by the transition λ to an absorbing state $\mathbf{\Omega}_a = \{1'\}$ in Fig. 2. Note that the overall absorbing state space includes both $\mathbf{\Omega_a}$ and $\mathbf{\Omega_0}$. The packet loss probability is then equal to the probability for the transient process in $\mathbf{\Omega_1}$ to be absorbed in $\mathbf{\Omega}_a$. Define such an absorbing probability conditioned on an entering state $X_i \in \mathbf{\Omega_1}$ by P_{ia}. We can have the *conditional Packet Loss Probability* column vector $\mathbf{p}_{CPL} = [P_{0a}\ P_{1a}\ \cdots\ P_{Ka}]^T$. Let $\mathbf{G}_1$ be the generator matrix of the transient-state birth-death process in $\mathbf{\Omega_1}$. Denote the transition rate vector from $\mathbf{\Omega_1}$ to $\mathbf{\Omega}_a$ by

$$\boldsymbol{\beta}_{1a} = [0\ 0\ \cdots\ 0\ \lambda]^T. \tag{6}$$

From (3), we get $\mathbf{p}_{CPL} = -\mathbf{G}_1^{-1}\boldsymbol{\beta}_{1a}$. Given the entering probability row vector $\boldsymbol{\alpha}_{in} = [\alpha_0\ \alpha_1\ \cdots\ \alpha_K]$ from $\mathbf{\Omega_1}$ to $\mathbf{\Omega_0}$, the unconditional packet loss probability is expressed by $L_p = \boldsymbol{\alpha}_{in}\mathbf{p}_{CPL}$, which leads to

$$L_p = -\boldsymbol{\alpha}_{in}\mathbf{G}_1^{-1}\boldsymbol{\beta}_{1a}, \tag{7}$$

and so the probability for packet to succeed is $P_g = 1 - L_p$. The overall steady state solution vector $\boldsymbol{\pi}$ in $\mathbf{\Omega}$ is also divided into two subvectors: $\boldsymbol{\pi^0} = [\pi_{00}\ \pi_{01}\ \cdots\ \pi_{0K}]$ for the steady state probabilities in $\mathbf{\Omega}_0$ and

$\boldsymbol{\pi^1} = [\pi_{10}\ \pi_{11}\ \cdots\ \pi_{1K}]$ for the steady state probabilities in $\boldsymbol{\Omega}_1$. Since each transition rate from $\boldsymbol{\Omega}_0$ to $\boldsymbol{\Omega}_1$ is constant α, we can get

$$\boldsymbol{\alpha}_{in} = \frac{\boldsymbol{\pi^0}\ \alpha\ \mathbf{I}}{\boldsymbol{\pi^0}\ \alpha\ \mathbf{e}} = \frac{\boldsymbol{\pi^0}}{\boldsymbol{\pi^0}\ \mathbf{e}}, \tag{8}$$

which is applied to (7) for the computation of L_p.

Define the average transmission time of each successful packet by S_g which is characterized by the overall mean sojourn time in $\boldsymbol{\Omega}_1$ under the condition for the transient process to be absorbed in $\boldsymbol{\Omega}_0$. Let $b_i = \sum_j b_{ij}$ be the probability for the transient process to be absorbed in $\boldsymbol{\Omega}_0$, conditioned on the entering state $(1,i) \in \boldsymbol{\Omega}_1$ for $i = 0, 1, ..., K$. According to (4), the conditional mean sojourn time column vector for the transient process to be absorbed in $\boldsymbol{\Omega}_0$ given the entering state $(1,i) \in \boldsymbol{\Omega}_1$ can be expressed by

$$\overline{\mathbf{t}}_g = -\mathbf{D}_0^{-1}\mathbf{G}_1^{-1}\mathbf{D}_0\mathbf{e},$$

where $\mathbf{D}_0 = \text{diag}\{b_0, b_1, ..., b_K\}$. For the computation of $\mathbf{B} = [b_{ij}]$, one can write from (3)

$$\mathbf{G}_1\mathbf{B} = -\boldsymbol{\beta}_{10}. \tag{9}$$

Here, $\boldsymbol{\beta}_{10}$ is the transition rate vector from $\boldsymbol{\Omega}_1$ to $\boldsymbol{\Omega}_0$, given by

$$\boldsymbol{\beta}_{10} = [\beta\ \beta\ \cdots\ \beta]^T. \tag{10}$$

For the computation of S_g, we need to further remove the entering state condition $(1,i)$ from $\overline{\mathbf{t}}_g$. That is, $S_g = \boldsymbol{\alpha}'_{in}\ \overline{\mathbf{t}}_g$ where $\boldsymbol{\alpha}'_{in}$ is the entering probability row vector in $\boldsymbol{\Omega}_1$ conditioned on the absorption in $\boldsymbol{\Omega}_0$. One can derive $\boldsymbol{\alpha}'_{in}$ from the unconditional entering probability row vector $\boldsymbol{\alpha}_{in}$, which is given by

$$\boldsymbol{\alpha}'_{in} = \frac{\boldsymbol{\alpha}_{in}\mathbf{D}_0}{\boldsymbol{\alpha}_{in}\mathbf{D}_0\mathbf{e}}.$$

We thus get

$$S_g = \frac{-\boldsymbol{\alpha}_{in}\mathbf{G}_1^{-1}\mathbf{D}_0\mathbf{e}}{\boldsymbol{\alpha}_{in}\mathbf{D}_0\mathbf{e}}, \tag{11}$$

which can be readily obtained from $\mathbf{G}_1$, $\boldsymbol{\alpha}_{in}$ and $\boldsymbol{\beta}_{10}$ by the generalized Folding algorithm.

Similarly, we define the average transmission time of each packet by S, which is directly identified from the following load balancing equation,

$$S = (1 - L_c)\beta^{-1}, \tag{12}$$

where β^{-1} is the average packet generation time of the source (i.e., the average source ON-period). Note that the definition of S excludes the blocked cells and the transmission time of each entirely blocked packet is zero.

A transmitted packet can be either successful or corrupted. Further define the average transmission time of each corrupted/blocked packet by S_b, which corresponds to the overall mean sojourn time in $\boldsymbol{\Omega}_1$ under the condition for the transient process to be absorbed in $\boldsymbol{\Omega}_a$. Therefore S_b can be derived from the following load balancing equation:

$$S = S_b L_p + S_g(1 - L_p). \tag{13}$$

Combining (12) and (13), we have the following load balancing equation.

$$1 = L_c + \beta S_g(1 - L_p) + \beta S_b L_p. \tag{14}$$

In this equation, $\beta S_g(1 - L_p)$ is the probability of cells belong to successful packets. The cell rate of good packets is therefore given by $\lambda_c = \overline{\gamma}\beta S_g(1 - L_p)$. Thus we have the following relationship for goodput:

$$\rho_g = \lambda_c/\mu = \rho\beta S_g(1 - L_p). \tag{15}$$

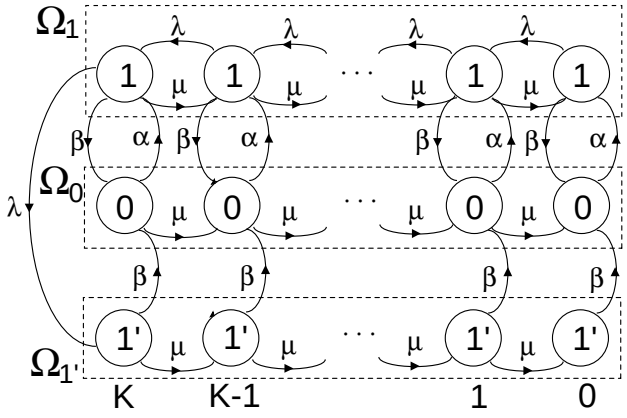

Figure 3: PTD modeling with a single source.

One can therefore derive ρ_g from S_g and L_p. The badput is simply given by $\rho_b = \rho(1 - L_c) - \rho_g$. Note that all solutions are readily obtained once $\mathbf{G}$, $\mathbf{G}_1$, $\boldsymbol{\alpha}_{in}$, $\boldsymbol{\beta}_{1a}$ and $\boldsymbol{\beta}_{10}$ are constructed for each particular packet discarding scheme, given that $\mathbf{G}$ and $\mathbf{G}_1$ have the QBD structure.

3.2 With Packet Tail Discarding

Once a cell in a packet is blocked due to buffer overflow, there will be no need to transmit its remaining cells. Otherwise, it wastes the network resources since a corrupted packet is equivalent to a lost packet at high layer protocols. In the PTD design, whenever the buffer becomes full, the remaining cell arrivals of each incoming packet will be discarded to prevent further congestion. In consequence, more buffer space and transmission bandwidth will be released to improve the transmission of other packets.

Similarly, one can derive L_p of the PTD scheme. In order to distinguish the noncorruption of a generated packet from the corruption while the source is ON, we further split the ON-period status into two phases: phase 1 for noncorruption and phase $1'$ for corruption as shown in Fig. 3. Similar to the previous case, the source turns on to generate a new packet each time upon the transition from phase 0 to phase 1 at rate α. If a cell is generated at rate λ when the buffer is full, the source will take the transition from phase 1 to phase $1'$ and from then on no cell arrivals of the packet will be accepted by the buffer till the end of the packet generation as described by the transition from phase $1'$ to phase 0 at rate β. Otherwise, the source remains in phase 1 during which all cell arrivals of the packet are accepted till the transition occurs from phase 1 to phase 0 at rate β, representing a successful packet generation. According to the source phases, we divide the entire state space $\boldsymbol{\Omega}$ of the involved queueing process into three subspaces: $\boldsymbol{\Omega}_0$, $\boldsymbol{\Omega}_1$ and $\boldsymbol{\Omega}_{1'}$, defined by $\boldsymbol{\Omega}_{\boldsymbol{i}} = \{(i,0),(i,1),...,(i,K)\}$ for $i = 0, 1, 1'$. Hence, each new packet generation starts by the transition from $\boldsymbol{\Omega}_0$ to $\boldsymbol{\Omega}_1$ at rate α. A successful packet generation is represented by the transition from $\boldsymbol{\Omega}_1$ to $\boldsymbol{\Omega}_0$ at rate β. A tail packet discarding starts by the transition from $\boldsymbol{\Omega}_1$ to $\boldsymbol{\Omega}_{1'}$ at rate λ when the buffer is full and terminates by the transition from $\boldsymbol{\Omega}_{1'}$ to $\boldsymbol{\Omega}_0$ at rate β as the packet generation terminates.

It is obvious that the involved queueing process is a finite QBD, whose five basic transition blocks $\mathbf{A}, \mathbf{D}, \mathbf{U}$, $\mathbf{A}_0$ and $\mathbf{A}_1$ for the generator matrix $\mathbf{G}$ in (1) are readily constructed from Fig. 3. The steady state solution $\boldsymbol{\pi}$ can be divided into three subvectors $\boldsymbol{\pi}^0$, $\boldsymbol{\pi}^1$ and $\boldsymbol{\pi}^{1'}$ with $\boldsymbol{\pi}^i = [\pi_{i0}\ \pi_{i1}\ \cdots\ \pi_{iK}]$ for $i = 0, 1$ and $1'$.

Since the transient process in $\boldsymbol{\Omega}_1$ is identical to the one defined in the previous subsection as shown in Fig. 2, all the $\mathbf{G}_1$, $\boldsymbol{\alpha}_{in}$, $\boldsymbol{\beta}_{1a}$ and $\boldsymbol{\beta}_{10}$ are unchanged here and so are the formulae for the computation of L_p, S_g and ρ_g. In this case, $\boldsymbol{\beta}_{1a}$ represents the transition rate vector from $\boldsymbol{\Omega}_1$ to $\boldsymbol{\Omega}_{1'}$ and given by the same

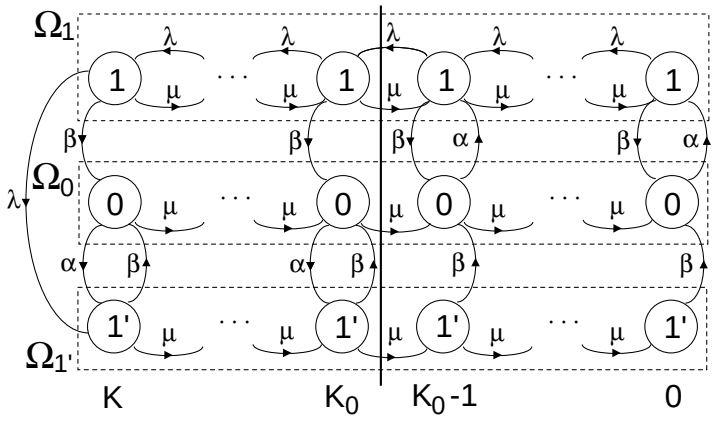

Figure 4: EPD modeling with a single source.

form as in (6).

3.3 With Early Packet Discarding

In the PTD scheme, cells in the front portion of each corrupted packet are still transmitted, which results in certain waste of buffer capacity and link bandwidth as measured by the badput ρ_b. In the EPD scheme, a decision is made at the beginning of each new packet generation based on the present queue congestion status. Cells of an entire packet will be discarded if the queue length $q(t)$ is greater than or equal to a queue congestion threshold K_0 at the beginning of the packet generation. Otherwise, they are all accepted unless the buffer is full after which the remaining cell arrivals are to be blocked as in the PTD scheme. A proper design of K_0 can detect early congestion and prevent further congestion by selective discarding, such that ρ_b is to be substantially reduced.

As shown by the state transition diagram in Fig. 4, the EPD scheme can be modeled by a QBD process with level dependent transitions, which is directly solvable by the Folding algorithm. For simplicity, the detail construction of the $\mathbf{G}$ matrix has been omitted. Similar to the PTD modeling, one can divide the state space $\mathbf{\Omega}$ into three subspaces: $\mathbf{\Omega}_0$, $\mathbf{\Omega}_1$ and $\mathbf{\Omega}_{1'}$. Each new packet generation starts by the transition from $\mathbf{\Omega}_0$ and $\mathbf{\Omega}_1$ at rate α in the buffer noncongestion period, i.e., $q(t) < K_0$. Otherwise, in the buffer congestion period, $q(t) \geq K_0$, each new packet generation is completely abandoned by the transition from $\mathbf{\Omega}_0$ and $\mathbf{\Omega}_{1'}$ at rate α. The rest transitions are identical to that of the PTD scheme. Note that the PTD scheme is a special case of the EPD scheme by taking $K_0 > K$.

Accordingly, the steady state solution $\boldsymbol{\pi}$ is divided into $\boldsymbol{\pi}^0$, $\boldsymbol{\pi}^1$ and $\boldsymbol{\pi}^{1'}$. We further decompose $\boldsymbol{\pi}^0$ into two subvectors: $\boldsymbol{\pi}^0_n = [\pi_{00}\ \pi_{01}\ \cdots\ \pi_{0(K_0-1)}]$ for noncongestion and $\boldsymbol{\pi}^0_c = [\pi_{0K_0}\ \pi_{0(K_0+1)}\ \cdots\ \pi_{0K}]$ for congestion. Denote the transition probability from $\mathbf{\Omega}_0$ to $\mathbf{\Omega}_1$ by p_{01} and from $\mathbf{\Omega}_0$ to $\mathbf{\Omega}_{1'}$ by $p_{01'}$, conditioned on each packet arrival. One can readily express

$$\begin{aligned} p_{01'} &= \frac{\boldsymbol{\pi}^0_c\ \alpha\ \mathbf{I}\ \mathbf{e}}{\boldsymbol{\pi}^0\ \alpha\ \mathbf{I}\ \mathbf{e}} = \frac{\boldsymbol{\pi}^0_c\ \mathbf{e}}{\boldsymbol{\pi}^0\ \mathbf{e}}, \\ p_{01} &= \frac{\boldsymbol{\pi}^0_n\ \mathbf{e}}{\boldsymbol{\pi}^0\ \mathbf{e}} = 1 - p_{01'}, \end{aligned} \tag{16}$$

where $\alpha\mathbf{I}$ is the transition rate matrix from $\mathbf{\Omega}_0$ to $\mathbf{\Omega}_1$, as well as from $\mathbf{\Omega}_0$ to $\mathbf{\Omega}_{1'}$ in proper dimension.

Obviously, conditioned on the transition from $\mathbf{\Omega}_0$ to $\mathbf{\Omega}_{1'}$, every new packet will be blocked. On the other hand, conditioned on the transition from $\mathbf{\Omega}_0$ to $\mathbf{\Omega}_1$, the probability for a new packet to be partially

discarded, denoted by L_t, is measured by the transition probability from $\mathbf{\Omega}_1$ to $\mathbf{\Omega}_{1'}$. The derivation of L_t is identical to that of L_p in the PTD scheme given by (7), except that $\mathbf{G}_1$ is defined on the subspace $\mathbf{\Omega}_1$ of the EPD scheme. Now, $\boldsymbol{\alpha}_{in}$ is given by

$$\boldsymbol{\alpha}_{in} = \frac{[\boldsymbol{\pi}_n^0 \ 0 \cdots 0]}{\boldsymbol{\pi}_n^0 \ \mathbf{e}} \tag{17}$$

since the transition from $\mathbf{\Omega}_0$ and $\mathbf{\Omega}_1$ is possible only during the buffer noncongestion period. The overall packet loss probability of the EPD scheme is then equal to

$$L_p = p_{01} \ L_t + p_{01'}, \tag{18}$$

where $p_{01} L_t$ is the probability for an arrival packet to be corrupted and $p_{01'}$ is the probability for an arrival packet to be entirely blocked. The average packet transmission time S is expressed in (12). Note that a packet can be either successfully transmitted, partially corrupted or entirely blocked. Since the average transmission time of successful, corrupted and blocked packet is given by S_g, S_b and 0, respectively, one can further decompose S into

$$S = S_b p_{01} \ L_t + S_g P_g.$$

The remaining computation of S_g and ρ_g is unchanged from the above two schemes and given by (11) and (15). The same $\boldsymbol{\beta}_{1a}$ and $\boldsymbol{\beta}_{10}$ as in (6) and (10) are used.

3.4 Extension to Window Flow Control

So far we have used the ON/OFF source modeling technique to characterize the individual packet generation. In reality, many data networks have adopted a window flow control mechanism for packet transport. Under the window flow control, the source will consecutively generate multiple packets within a given window size; it will then stop and wait for the acknowledgement from destination before to start the next window transmission. For simplicity, here we use a two-state Markov chain to model the alternation of window transmission period (ON-period) and waiting period (OFF-period), with respect to the rate β_w and α_w shown in Fig. 5. To characterize the consecutive packet generation within each window, we further decompose the ON-state into two alternating sub-ON states. Each transition between the two sub-ON states represents the termination of a packet generation within the window, as shown by β in Fig. 5. The average size of each packet is equal to β^{-1}, except for the last packet of each window which is terminated by the window at rate β_w. In other words, due to the modeling limitation we have assumed that the average size of the last packet within each window is different from the other packets. Such an assumption has negligible impact on the performance when the window size is significantly large. The overall average packet generation time is therefore given by $(\beta + \beta_w)^{-1}$. Without loss of generality, in Fig. 5 we also have assumed that a window is equally likely to start in each sub-ON state as shown by the transition rate $\alpha_w/2$.

We first consider the case without packet discarding. Its queueing system under the window flow control can be modeled by a regular QBD process, whose state space is defined by $\mathbf{\Omega} = \{\mathbf{\Omega}_0, \mathbf{\Omega}_{1_a}, \mathbf{\Omega}_{1_b}\}$ with $\mathbf{\Omega}_i = \{(i,0),(i,1),...,(i,K)\}$ for $i = 0, 1_a$, and 1_b, as shown by the transition diagram in Fig. 6. Accordingly, the steady state solution vector $\boldsymbol{\pi}$, derived from (2), is divided into three subvectors $\boldsymbol{\pi}^i = [\pi_{i0} \ \pi_{i1} \ \cdots \ \pi_{iK}]$ for $i = 0, 1_a$, and 1_b. The cell loss probability L_c is then expressed by

$$L_c = \frac{\lambda}{\overline{\lambda}}(\pi_{1_a K} + \pi_{1_b K}), \tag{19}$$

where $\overline{\lambda} = \frac{\alpha_W \lambda}{\alpha_W + \beta_W}$ is the average cell arrival rate. Since both sub-ON states are identical, we only need to focus on the transient process in $\mathbf{\Omega}_{1_a}$ upon the transition from $\mathbf{\Omega}_0$ or $\mathbf{\Omega}_{1_b}$ for the computation of P_g and ρ_g. A packet transmission starts either by the transition from $\mathbf{\Omega}_0$ to $\mathbf{\Omega}_{1_a}$ at rate $\alpha_w/2$ as the first packet

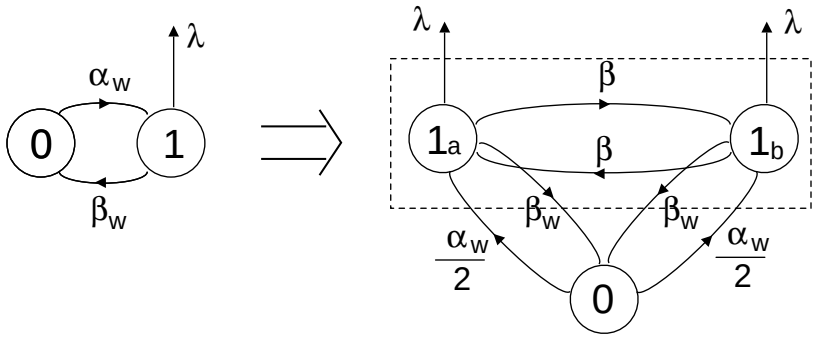

Figure 5: Source extension to window flow control.

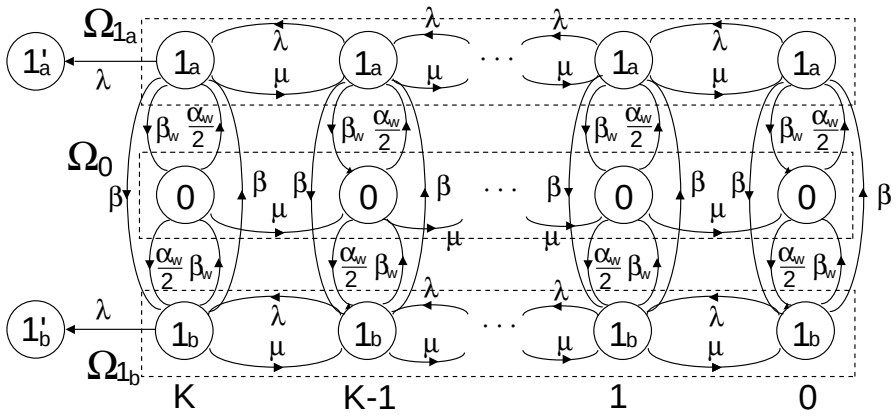

Figure 6: Transition diagram of window flow control.

in the window, or by the transition from $\mathbf{\Omega}_{1_b}$ to $\mathbf{\Omega}_{1_a}$ at rate β as the rest of packets in the window. It can terminate successfully by the transition from $\mathbf{\Omega}_{1_a}$ to $\mathbf{\Omega}_0$ at rate β_W as the last packet within the window, or by the transition from $\mathbf{\Omega}_{1_a}$ to $\mathbf{\Omega}_{1_b}$ at rate β as any other packet within the window. Yet, it can also be corrupted by the transition from $\mathbf{\Omega}_{1_a}$ to the absorbing state $1'_a$ at rate λ upon a cell arrival when the buffer is full.

Accordingly, the entering probability vector $\boldsymbol{\alpha}_{_{in}}$ from $\mathbf{\Omega}_0$ or $\mathbf{\Omega}_{1_b}$ to $\mathbf{\Omega}_{1_a}$ becomes

$$\boldsymbol{\alpha}_{_{in}} = \frac{\boldsymbol{\pi}^{\mathbf{0}} \frac{\alpha_W}{2} + \boldsymbol{\pi}^{\mathbf{1_b}} \beta}{\boldsymbol{\pi}^{\mathbf{0}} \frac{\alpha_W}{2} \mathbf{e} + \boldsymbol{\pi}^{\mathbf{1_b}} \beta \mathbf{e}},$$

which replaces (8) for the computation of L_p in (7). Similarly, we need to redefine $\boldsymbol{\beta}_{_{10}}$ by

$$\boldsymbol{\beta}_{_{10}} = [\beta + \beta_W \;\; \beta + \beta_W \;\; \cdots \;\; \beta + \beta_W]^T$$

for the transitions from $\mathbf{\Omega}_{1_a}$ to $\mathbf{\Omega}_{1_b}$ or $\mathbf{\Omega}_0$. The rest of the computations for P_g, ρ_g, and ρ_b remain unchanged as in Section 3.1 except to replace β by $\beta + \beta_W$ in (12) and $\mathbf{G}_1$ by $\mathbf{G}_{1a}$ for the transition rate matrix in $\mathbf{\Omega}_{1_a}$.

Similarly, P_g and ρ_g of the PTD and EPD schemes can be found by defining a new state space $\mathbf{\Omega} = \{\mathbf{\Omega}_0, \mathbf{\Omega}_{1_a}, \mathbf{\Omega}_{1_b}, \mathbf{\Omega}_{1'}\}$ with $\mathbf{\Omega}_i = \{(i,0),(i,1),...,(i,K)\}$ for $i = 0, 1_a, 1_b$, and $1'$. The transition rates among $0, 1_a, 1_b$ and $1'$ at each queue level are readily obtainable for each given scheme. The same techniques used in Sections 3.2 and 3.3 can then be applied to find the solutions.

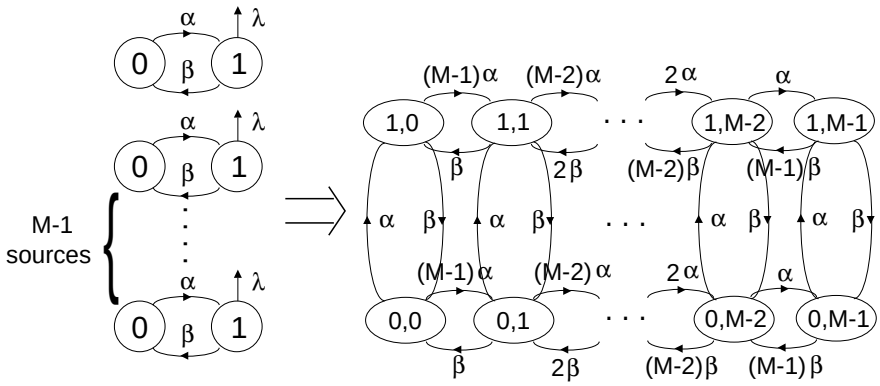

Figure 7: Grouping of $(M-1)$ 2-state sources.

4 Modeling with Multiple ON/OFF Sources

The extension of the above single-source modeling to multi-source modeling is achieved by state space grouping. For each scheme, once we construct the grouped $\mathbf{G}$, $\mathbf{G}_1$, $\boldsymbol{\alpha}_{in}$, $\boldsymbol{\beta}_{1a}$ and $\boldsymbol{\beta}_{10}$ the basic computation for L_c, L_p, S_g and ρ_g remains unchanged as in the single source case.

4.1 Without Packet Discarding

Consider M homogeneous ON/OFF sources. Since all the sources are equally treated with FIFO service scheduling, the statistical performance experienced by every source must be i.i.d. In other words, one can simply take a marked source for performance analysis while grouping the remaining $(M-1)$ sources. The grouped $(M-1)$ sources are modeled by a birth-death process whose transition rate matrix $\mathbf{Q}_{gp} = [q_{jl}]$ is defined by

$$q_{jl} = \begin{cases} (M-1-j)\alpha, & \text{if } l = j+1, \\ -(M-1-j)\alpha - j\beta & \text{if } l = j, \\ j\beta, & \text{if } l = j-1, \\ 0, & \text{otherwise.} \end{cases} \tag{20}$$

Then, taking the superposition of the marked source with the grouped sources, we get a two-dimensional Markov chain as described in Fig. 7 with each phase defined by (i,j) where $i = 0, 1$ for the marked source and $j = 0, 1, ..., M-1$ for the grouped sources. Its transition rate matrix is expressed by

$$\mathbf{Q} = \begin{bmatrix} \mathbf{Q}_{gp} - \alpha\mathbf{I} & \alpha\mathbf{I} \\ \beta\mathbf{I} & \mathbf{Q}_{gp} - \beta\mathbf{I} \end{bmatrix} \tag{21}$$

and the corresponding arrival rate matrix by

$$\boldsymbol{\Gamma} = \begin{bmatrix} \boldsymbol{\Gamma}_0 & \mathbf{0} \\ \mathbf{0} & \boldsymbol{\Gamma}_1 \end{bmatrix}, \tag{22}$$

where $\boldsymbol{\Gamma}_0 = \text{diag}[0, \lambda, 2\lambda, ..., (M-1)\lambda]$ is the arrival rate submatrix while the marked source is in OFF state. $\boldsymbol{\Gamma}_1 = \boldsymbol{\Gamma}_0 + \lambda\mathbf{I}$ is the arrival rate submatrix while the marked source is in ON state. The five basic blocks of $\mathbf{G}$ matrix in (1) of the QBD modeling are then expressed as $\mathbf{D} = \mu\mathbf{I}$, $\mathbf{U} = \boldsymbol{\Gamma}$, $\mathbf{A} = \mathbf{Q} - \mathbf{D} - \mathbf{U}$, $\mathbf{A}_0 = \mathbf{Q} - \mathbf{U}$, and $\mathbf{A}_1 = \mathbf{Q} - \mathbf{D}$. The steady state solution vector $\boldsymbol{\pi}$ is readily obtained from $\boldsymbol{\pi}\mathbf{G} = \mathbf{0}$. Similar to the single source QBD modeling, we can divide the entire QBD state space $\boldsymbol{\Omega}$ into two disjoint

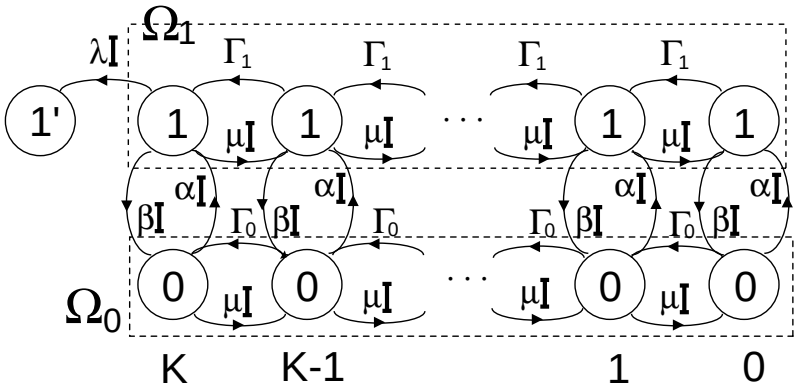

Figure 8: Modeling of no packet discarding with multiple sources.

sets: $\mathbf{\Omega}_0$ for the marked source in OFF state and $\mathbf{\Omega}_1$ for the marked source in ON state. Accordingly, the steady state solution vector $\boldsymbol{\pi}$ is divided into $\boldsymbol{\pi}^0$ for $\mathbf{\Omega}_0$ and $\boldsymbol{\pi}^1$ for $\mathbf{\Omega}_1$.

The generator matrix $\mathbf{G}_1$ for the transient-state QBD defined on $\mathbf{\Omega}_1$ is constructed by $\mathbf{D} = \mu\mathbf{I}$, $\mathbf{U} = \mathbf{\Gamma}_1$, $\mathbf{A} = \mathbf{Q}_{gp} - \beta\mathbf{I} - \mathbf{D} - \mathbf{U}$, $\mathbf{A}_0 = \mathbf{Q} - \beta\mathbf{I} - \mathbf{U}$, and $\mathbf{A}_1 = \mathbf{A}$, as shown in Fig. 8. Define an absorbing state subspace of this transient-state QBD by $\mathbf{\Omega}_a = \{(i,j,k) \mid i = 1, \forall j, k = K\}$. The transition from $\mathbf{\Omega}_1$ to $\mathbf{\Omega}_a$ is given by

$$\boldsymbol{\beta}_{1a} = [\overbrace{\mathbf{0} \cdots \mathbf{0}}^{K} \ \boldsymbol{\lambda}]^T, \tag{23}$$

where $\mathbf{0}$ is a zero vector of dimension M for nonexisting transition at each buffer level (except K) and $\boldsymbol{\lambda} = \lambda\mathbf{e}^T$ is for existing transition from buffer level K to $\mathbf{\Omega}_a$. Similarly, the transition from $\mathbf{\Omega}_1$ to $\mathbf{\Omega}_0$ is given by

$$\boldsymbol{\beta}_{10} = [\boldsymbol{\beta} \ \boldsymbol{\beta} \ \cdots \ \boldsymbol{\beta}]^T, \tag{24}$$

where $\boldsymbol{\beta} = [\beta \ \beta \ \cdots \ \beta]$ is for transition from $\mathbf{\Omega}_1$ to $\mathbf{\Omega}_0$ at each queue level. The initial state probability vector of $\mathbf{\Omega}_1$ is expressed by

$$\boldsymbol{\alpha}_{in} = [\ \boldsymbol{\alpha}_0 \ \boldsymbol{\alpha}_1 \ \cdots \ \boldsymbol{\alpha}_K \ ], \tag{25}$$

where $\boldsymbol{\alpha}_i$ is the initial state probability subvector on queue level i in $\mathbf{\Omega}_1$. As in the single-source case,

$$\boldsymbol{\alpha}_{in} = \frac{\boldsymbol{\pi}^0\alpha\mathbf{I}}{\boldsymbol{\pi}^0\alpha\mathbf{e}} = \frac{\boldsymbol{\pi}^0}{\boldsymbol{\pi}^0\mathbf{e}}. \tag{26}$$

4.2 With Packet Tail Discarding

In the PTD modeling, each source consists of three phases $\{0, 1, 1'\}$. By the superposition of $(M-1)$ such i.i.d. sources, the grouped state can be expressed by $(n_0, n_1, n_{1'})$ where n_i represents the number of sources in phase i. Since $n_0 + n_1 + n_{1'} = M - 1$, one can simply define $(n_1, n_{1'})$ as the state of the grouped sources for Markov chain modeling. For the grouping of $(M-1)$ sources, one can express its transition rate matrix as $\mathbf{Q}_{gp} = [q_{(n_1,n_{1'})(m_1,m_{1'})}]$ by

$$q_{(n_1,n_{1'})(m_1,m_{1'})} = \begin{cases} n_{1'}\beta & \text{if } m_1 = n_1 \text{ and } m_{1'} = n_{1'} - 1, \\ n_1\beta & \text{if } m_1 = n_1 - 1 \text{ and } m_{1'} = n_{1'}, \\ (M - 1 - n_1 - n_{1'})\alpha & \text{if } m_1 = n_1 + 1 \text{ and } m_{1'} = n_{1'}, \\ -(i+j)(\beta - \alpha) - (M-1)\alpha & \text{if } m_1 = n_1 \text{ and } m_{1'} = n_{1'} \\ 0 & \textit{otherwise}. \end{cases} \tag{27}$$

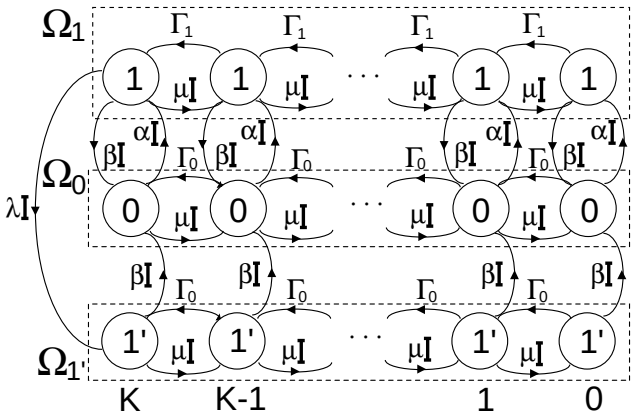

Figure 9: PTD modeling with multiple sources.

We then superimpose the marked source with the grouped sources to form a new Markov chain described by

$$\mathbf{Q} = \begin{bmatrix} \mathbf{Q}_{gp} - \beta\mathbf{I} & \beta\mathbf{I} & \mathbf{0} \\ \mathbf{0} & \mathbf{Q}_{gp} - \alpha\mathbf{I} & \alpha\mathbf{I} \\ \mathbf{0} & \beta\mathbf{I} & \mathbf{Q}_{gp} - \beta\mathbf{I} \end{bmatrix}. \tag{28}$$

When the buffer becomes full, an incoming cell from a source makes that source inactive, *i.e.*, all the remaining cells from the source will be blocked. For grouped sources this process can be explained by the following transition

$$q_{(n_1,n_{1'})(m_1,m_{1'})} = n_1\lambda, \qquad \text{if } m_1 = n_1 - 1 \text{ and } m_{1'} = n_{1'} + 1. \tag{29}$$

By adding this transition to (27), we can modify $\mathbf{Q}_{gp}$ to a new transition rate matrix $\mathbf{Q}'_{gp}$ at buffer level K. Denote $\mathbf{Q}$ in (28) by $\mathbf{Q}'$ after making the replacement of $\mathbf{Q}_{gp}$ by $\mathbf{Q}'_{gp}$.

The diagonal arrival rate matrix while the marked source is in phase i is denoted by $\mathbf{\Gamma}_i = \text{diag}_{n_1,n_{1'}}\{\gamma^i_{(n_1,n_{1'})}\}$ for $i = 0, 1, 1'$. Since only the sources in phase 1 will generate packet, we get $\gamma^0_{(n_1,n_{1'})} = n_1\lambda$, $\gamma^1_{(n_1,n_{1'})} = (n_1+1)\lambda$ and $\gamma^{1'}_{(n_1,n_{1'})} = n_1\lambda$. Hence,

$$\mathbf{\Gamma} = \begin{bmatrix} \mathbf{\Gamma}_1 & \mathbf{0} & \mathbf{0} \\ \mathbf{0} & \mathbf{\Gamma}_0 & \mathbf{0} \\ \mathbf{0} & \mathbf{0} & \mathbf{\Gamma}_{1'} \end{bmatrix}. \tag{30}$$

Fig. 9 shows the state transition diagram of the PTD scheme with multiple sources. The five basic blocks of the $\mathbf{G}$ matrix are then expressed by $\mathbf{D} = \mu\mathbf{I}$, $\mathbf{U} = \mathbf{\Gamma}$, $\mathbf{A} = \mathbf{Q} - \mathbf{D} - \mathbf{U}$, $\mathbf{A}_0 = \mathbf{Q} - \mathbf{U}$, and $\mathbf{A}_1 = \mathbf{Q}' - \mathbf{D} - \mathbf{F}$, where $\mathbf{F}$ is a submatrix to take into account the transition from $\mathbf{\Omega}_1$ to $\mathbf{\Omega}_{1'}$ when the buffer is full, given by

$$\mathbf{F} = \begin{bmatrix} -\lambda\mathbf{I} & \mathbf{0} & \lambda\mathbf{I} \\ \mathbf{0} & \mathbf{0} & \mathbf{0} \\ \mathbf{0} & \mathbf{0} & \mathbf{0} \end{bmatrix}. \tag{31}$$

The transient process structure in $\mathbf{\Omega}_1$ is identical to the one in the previous subsection. Hence, all the structures of $\mathbf{G}_1$, $\boldsymbol{\alpha}_{in}$, $\boldsymbol{\beta}_{1a}$ and $\boldsymbol{\beta}_{10}$ remain unchanged and so do the solution forms for L_p, S_g and ρ_g.

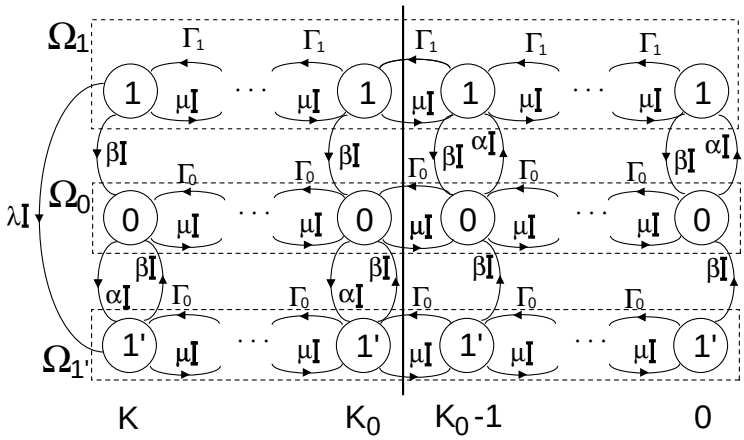

Figure 10: EPD modeling with multiple sources.

4.3 With Early Packet Discarding

The source grouping in the EPD modeling needs to be divided into the grouping in congestion period ($q(t) \geq K_0$) and the grouping in noncongestion period ($q(t) < K_0$). The grouping in noncongestion period is exactly identical to that in the PTD modeling as given by (27), (28) and (30). The grouping in congestion period leads to

$$\mathbf{Q}_c = \begin{bmatrix} \mathbf{Q}_{gpc} - \beta\mathbf{I} & \beta\mathbf{I} & \mathbf{0} \\ \alpha\mathbf{I} & \mathbf{Q}_{gpc} - \alpha\mathbf{I} & \mathbf{0} \\ \mathbf{0} & \beta\mathbf{I} & \mathbf{Q}_{gpc} - \beta\mathbf{I} \end{bmatrix}, \tag{32}$$

where $\mathbf{Q}_{gpc} = [q_{(n_1,n_{1'})(m_1,m_{1'})}]$ is the transition rate matrix for the grouping of $(M-1)$ sources in congestion period, expressed by

$$q_{(n_1,n_{1'})(m_1,m_{1'})} = \begin{cases} n_{1'}\beta & \text{if } m_1 = n_1 \text{ and } m_{1'} = n_{1'} - 1, \\ n_1\beta & \text{if } m_1 = n_1 - 1 \text{ and } m_{1'} = n_{1'}, \\ (M-1-n_1-n_{1'})\alpha & \text{if } m_1 = n_1 \text{ and } m_{1'} = n_{1'} + 1, \\ -(i+j)(\beta-\alpha) - (M-1)\alpha & \text{if } m_1 = n_1 \text{ and } m_{1'} = n_{1'} \\ 0 & \textit{otherwise}. \end{cases} \tag{33}$$

The aggregate arrival rate matrix in congestion period is identical to that in noncongestion period as denoted by $\mathbf{\Gamma}$ in (30). At buffer level K, the transition rate matrix $\mathbf{Q}_{gpc}$ in (33) is changed to a new transition rate matrix $\mathbf{Q}'_{gpc}$ by the inclusion of the transitions in (29). Then the transition rate matrix $\mathbf{Q}_c$ in (32) is also modified to a new transition rate matrix $\mathbf{Q}'_c$ with the replacement of $\mathbf{Q}_{gpc}$ by $\mathbf{Q}'_{gpc}$. Fig. 10 displays the QBD transition diagram of the EPD scheme with multiple sources, whose $\mathbf{G}$ matrix is represented by

$$\mathbf{G} = \begin{bmatrix} \mathbf{A}_0 & \mathbf{U} & & & & & & \\ \mathbf{D} & \mathbf{A} & \mathbf{U} & & & & & \\ & \ddots & \ddots & \ddots & & & & \\ & & \mathbf{D} & \mathbf{A} & \mathbf{U} & & & \\ & & & \mathbf{D} & \mathbf{A}_c & \mathbf{U} & & \\ & & & & \ddots & \ddots & \ddots & \\ & & & & & \mathbf{D} & \mathbf{A}_c & \mathbf{U} \\ & & & & & & \mathbf{D} & \mathbf{A}_1 \end{bmatrix}, \tag{34}$$

with $\mathbf{A}_c = \mathbf{Q}_c - \mathbf{D} - \mathbf{U}$ and $\mathbf{A}_1 = \mathbf{Q}'_c - \mathbf{D} - \mathbf{F}$. The rest blocks are in the same form as in the PTD modeling. Further, the $\mathbf{G}_1$ matrix for the transient process in $\mathbf{\Omega}_1$ is identical to that of the PTD modeling. Similar to the single-source EPD modeling, the steady state solution $\boldsymbol{\pi}$ is divided into $\boldsymbol{\pi}^0$, $\boldsymbol{\pi}^1$ and $\boldsymbol{\pi}^{1'}$ based on the state space division $\mathbf{\Omega}_0$, $\mathbf{\Omega}_1$ and $\mathbf{\Omega}_{1'}$. The solution $\boldsymbol{\pi}^0$ is further decomposed into $\boldsymbol{\pi}^0_c$ and $\boldsymbol{\pi}^0_n$ for congestion and noncongestion periods. One can then use (16), (17) and (18) for the computation of L_p. Both $\boldsymbol{\beta}_{1a}$ and $\boldsymbol{\beta}_{10}$ are in the same form as the PTD modeling.

4.4 Extension to Window Flow Control

The same source grouping technique can be readily applied to the window flow control analysis of multiple sources for different packet discarding schemes.

5 Performance Evaluation

Since few studies of data packet performance in ATM systems are available to date, it is important to systematically examine the impact of various design/control parameters and source characteristics on the packet transmission behavior as measured by P_g, ρ_g and ρ_b. This is achieved in this section by numerical study based on the above analyses. Our objectives are to compare the performance of the three schemes (noncontrolled, PTD and EPD) and to identify those system design/control factors which have substantial impact on the performance.

Based on the ON/OFF source modeling for packet generation, the average size of each generated packet is $\lambda\beta^{-1}$ and the average cell arrival rate of each source is $\lambda\alpha/(\alpha+\beta)$. For the superposition of M i.i.d. sources, the overall cell arrival rate is then given by

$$\overline{\gamma} = M\lambda\frac{\alpha}{\alpha+\beta}.$$

Note that one can identify α from $\overline{\gamma}$, M and β for the ON/OFF source modeling. In the simulation study by *Floyd* and *Romanov* [3], various packet sizes were selected: 512 bytes for IP networks, 1500 bytes for ethernet; 4352 bytes for FDDI; and 9180 bytes for IP over ATM. Here we choose three average packet sizes: 5KB, 10KB, and 20KB. For most studies, we will use the packet size 10KB unless otherwise noted.

We consider a single ATM link with capacity of $\mu = 155$Mbps. A finite buffer capacity K is selected from $\{2^8,\ 2^9,\ 2^{10},\ 2^{11},\ 2^{12}\}$ defined in ATM cell units. The cell loading factor $\rho = \overline{\gamma}/\mu$ changes in the range of $[0.5,\ 4.0]$, where we choose $\rho > 1$ to represent an overload period during which a large portion of the packet transmissions could fail as studied in [5]. Unless otherwise stated, we assume $M = 10$ sources (virtual connections) on the link.

In Section 5.1 we investigate the effect of system design factors ρ, K, and K_0 (queue threshold) on the data performance. Section 5.2 examines the impact of source control factors λ, β, and M. Section 5.3 considers heterogeneous sources. Section 5.4 studies window flow control performance. Section 5.5 evaluates the data performance with high-priority real-time traffic transmission. It should be pointed out that the following solutions derived in each case have been verified by computer simulation.

5.1 Effect of System Design Factors

Let us first examine the effect of buffer capacity K. Consider a system loaded at $\rho = 0.9$ to support $M = 10$ sources. The cell generation rate of each packet while a source in ON is defined at $\lambda = \mu/2$. Hence, the maximum cell arrival rate, which occurs while all the sources are ON, is five times of the link transmission rate. The average size of 10KB per packet is selected. In Fig. 11 we compare the performance of P_g, ρ_g, and ρ_b of the three packet discarding schemes as a function of K. In the design of EPD scheme, we have

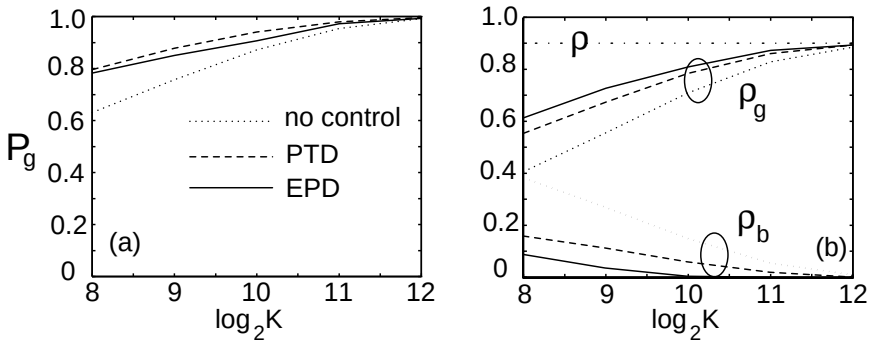

Figure 11: Effect of K on (a) P_g; (b) ρ_g and ρ_b.

set the queue threshold at $K_0 = K/2$ for each given K. As one can see, all the performance measurements improve as K increases. For small buffer size $K = 2^8$, the goodput ρ_g is only 40% for noncontrolled scheme but reaching about 55% for PTD and 60% for EPD. Notice $\rho_b = \rho(1 - L_c) - \rho_g$ for the badput, which is significant. As K increases, the difference among the three schemes gradually reduces. For moderate buffer size $K = 2^{10}$, ρ_b approaches to 0 for EPD but still remains at 10% and 20% for PTD and noncontrolled scheme. It is obvious that EPD and PTD always achieve better performance than noncontrolled scheme. Further, while the ρ_g of EPD is always better than that of PTD, its P_g is slightly less than that of PTD. This is because shorter packets in PTD are more likely to be successfully transmitted than longer ones. This is verified by the fact that the S_g of PTD is always less than that of EPD. In other words, although EPD may transmit less number of good packets than PTD, its actual cell throughput of the good packets is always greater than that of PTD.

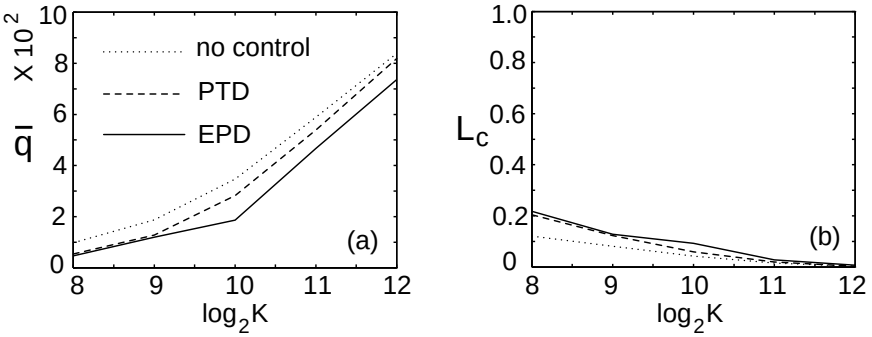

Figure 12: Effect of K on (a) $\overline{q}$; (b) L_c.

In Fig. 12 we further inspect the cell performance of the three schemes as measured by the cell loss rate L_c and average queue length $\overline{q}$. Among the three schemes, the noncontrolled system has achieved the best cell loss rate with the worst queueing performance. This is because more cells of corrupted packets are accepted by the noncontrolled scheme. Comparatively, the PTD system achieves higher cell loss rate with better queue length by the tail discarding of corrupted packets. In contrast, using early packet discarding the EPD scheme achieves the worst cell loss rate with the best queueing performance. As one can see, if the data performance were merely measured by the cell loss rate, one would claim that the noncontrolled system has the best performance while the EPD is the worst one, which is completely opposite to the previous observation based on the packet level measurement.

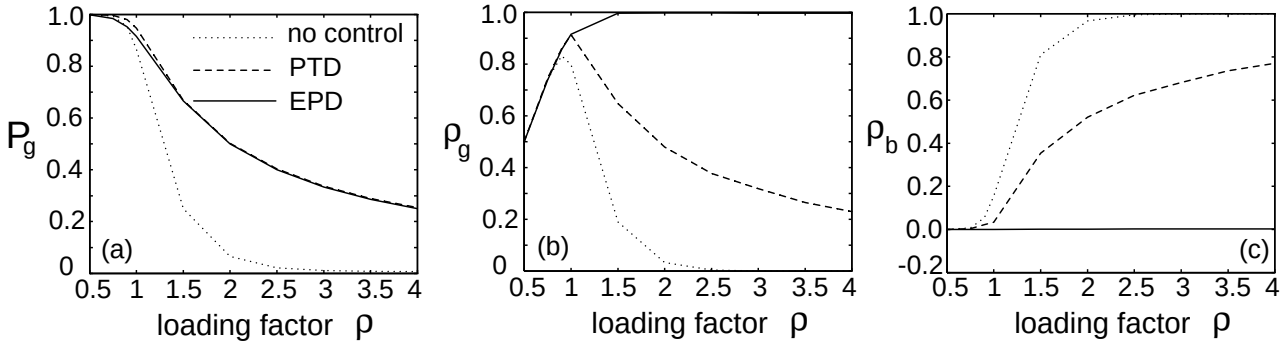

Figure 13: Effect of ρ on (a) P_g; (b) ρ_g; (c) ρ_b.

Next, we study the effect of loading factor ρ. Since network system engineers are more interested in the performance of packet discarding schemes when the system is overloaded [5], one may purposely increase ρ greater than 1 to reflect the overload condition. Let us change the loading condition in the range of $\rho \in [0.5,\ 4.0]$, i.e., in the worst cast the average cell arrival rate $\overline{\gamma}$ is four times of the link transmission rate μ. Note that the finite-buffer system is always stable for $\rho > 1$ while the achieved cell throughput $\rho_g + \rho_b$ can never exceed 1. We set $K = 2^{11}$ for buffer capacity and $K_0 = K/2$ for EPD. The cell arrival rate of each source is fixed at $\lambda = \mu/2$ with 10 i.i.d. sources. The change of ρ is therefore achieved through the adjustment of OFF-period at each source. Displayed in Fig. 13 are the results of P_g, ρ_g and ρ_b of the three schemes as a function of ρ. One critical observation is the rapid decline of ρ_g approaching to zero in the noncontrolled system as ρ increases. In other words, fewer packets can be successfully transmitted when the system is more overloaded without control. A similar trend can be found for PTD although its ρ_g is not close to zero. The study explores a nonstable phenomenon which can drastically reduce the goodput or even shut down the entire system unless some proper high layer flow control protocols are designed to pull the system out of the overload condition. In fact, such an accelerated congestion situation can get much worse since a large number of corrupted packets, departed from this node and measured by ρ_b, can not be detected by the downstream nodes and so they will stay within the network till reaching their destinations. In contrast, the goodput of EPD always tends to increase and approach to 1 while its badput is always close to 0 as ρ increases.

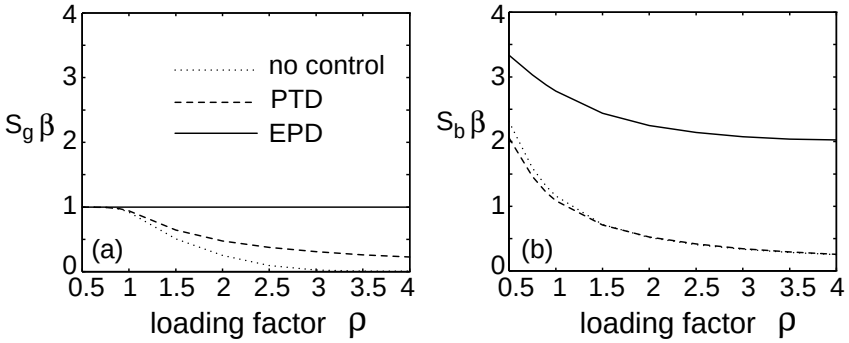

Figure 14: Packet size variation: (a) good packets; (b) bad packets.

While the goodput of EPD is always significantly better than that of PTD, one may find in Fig. 13 that both PTD and EPD have achieved about the same P_g performance. Again, this is because the average size

of success packets is much shorter for PTD than that for EPD. Plotted in Fig. 14 are the corresponding average size of success packets and corrupted packets of the three schemes, as proportionally measured by S_g and S_b, respectively. For convenience, both S_g and S_b are normalized by the average packet generation time β^{-1}. $S_g\beta \leq 1$ indicates that the average size of success packets cannot be greater than the average size of generated packets. For EPD, S_g is close to β^{-1} and basically unaffected by ρ. For PTD and noncontrolled, S_g rapidly reduces as ρ increases, indicating that success packets are getting shorter and shorter as the overload condition deteriorates. The lower ρ_b and higher $S_b\beta$ for EPD implies that only a few of longer packets are likely to be corrupted.

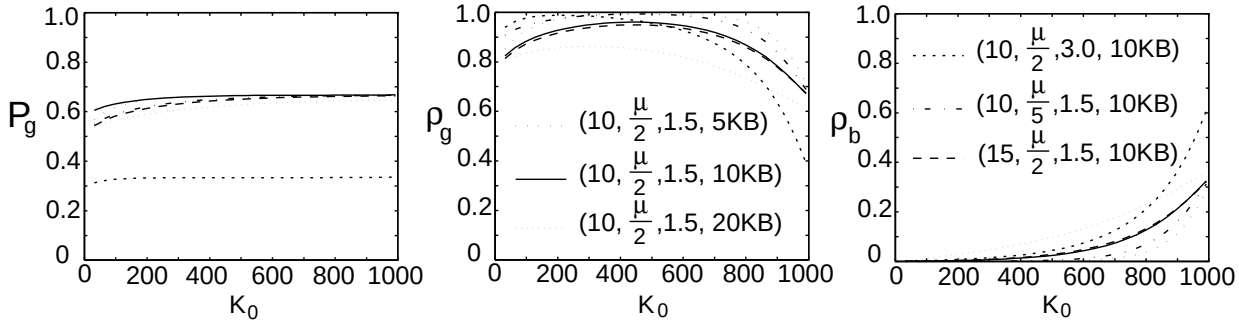

Figure 15: Effect of K_0 on EPD performance: (a) P_g; (b) ρ_g; (c) ρ_b.

Let us now examine the effect of buffer control threshold K_0 on EPD performance; we fixed K at 2^{10} but change K_0 over the range [32, 992]. In the first case, we set $\lambda = \mu/2$, $\rho = 1.5$ and $\lambda\beta^{-1} = 10$KB. The number of connection is set to $M = 10$. The solutions (P_g, ρ_g, ρ_b) are plotted in Fig. 15. As one can see, there exists an optimal solution $K_0 = 448$ for the maximum ρ_g. Also as expected, the badput ρ_b increases with K_0 since more packets are corrupted at a higher threshold, especially when $K_0 > 448$ which leads to the decline of ρ_g. On the other hand, P_g is always improved as K_0 increases, especially when $K_0 < 448$, since more packets are likely accepted and successfully transmitted. The study indicates the importance of selecting a right control threshold.

In order to observe the sensitivity of the optimal selection of K_0, we further change K_0 along with the following variations: for packet size $\lambda\beta^{-1} \in \{5\text{KB},\ 10\text{KB},\ 20\text{KB}\}$, at loading factor $\rho \in \{1.5,\ 3.0\}$, the burstiness $\lambda = \{\mu/5,\ \mu/2\}$, and the number of connections $M \in \{10,\ 15\}$. The solutions are also plotted in Fig. 15 and it is clearly shown that K_0 is not significantly sensitive to parameter variations.

5.2 Effect of Source Control Factors

In this subsection we focus on the effect of source control factors such as the average packet (burst) size $\lambda\beta^{-1}$, the source peak cell arrival rate λ, and the number of sources M. Some of these factors, such as the average packet size, may vary significantly for different applications. Other factors, such as λ and M, may be controllable by network protocols. To emphasize on the overload performance, we choose $\rho = 2$. The noncontrolled system shall not be considered here since its performance collapses at this loading. Describe the source characteristics by $\lambda = \mu/2$, $\lambda\beta^{-1}$=10KB and $M = 10$, among which one of them will be adjusted in each study.

We first adjust the source peak cell arrival rate $\lambda \in \{\mu, \frac{\mu}{2}, \frac{\mu}{4}\}$, which in the worst case is equal to the full transmission rate. Since the packet size $\lambda\beta^{-1}$ is fixed, the average ON-period (burst duration) of each source, β^{-1}, will be inversely proportional to λ and therefore adjusted accordingly. Again, we set $K_0 = K/2$ for EPD. Fig. 16a shows the EPD performance of P_g, ρ_g and ρ_b with respect to the three different λ's as

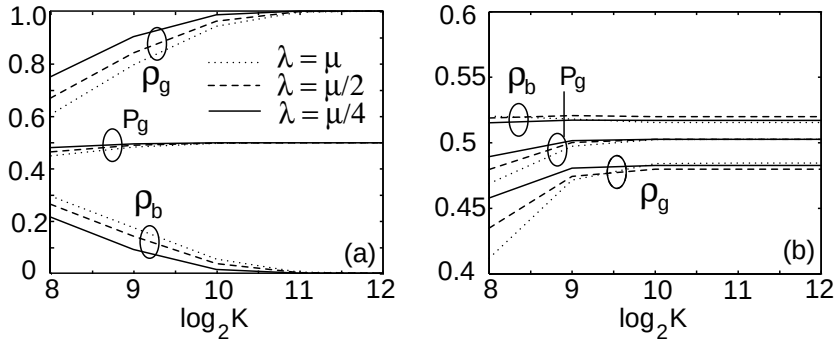

Figure 16: Effect of λ on (P_g, ρ_g, ρ_b): (a) EPD; (b) PTD.

a function of K. The performance always deteriorates as λ increases because the traffic becomes burstier. Such a deterioration gets less significant as K increases. Note $P_g \to \frac{1}{\rho}$ for large buffer size as expected. As shown in Fig. 16b, the performance of PTD is improved by increasing λ, especially for small buffer size. Yet, as compared to EPD, its improvement is much less significant, especially when $K \geq 2^9$.

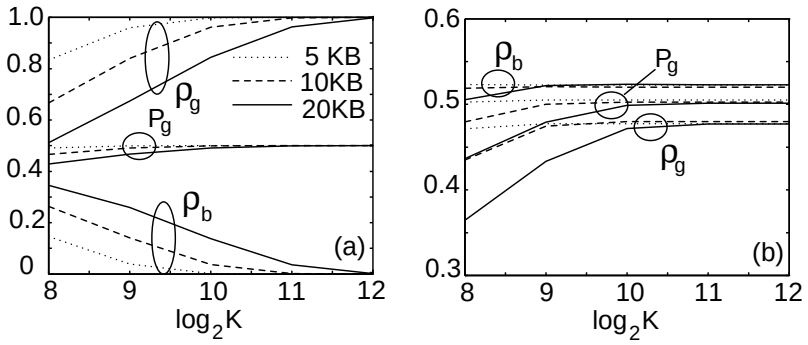

Figure 17: Effect of average packet size on (P_g, ρ_g, ρ_b): (a) EPD; (b) PTD.

Next, we inspect the effect of the average packet (burst) size $\lambda\beta^{-1} \in \{5KB,\ 10KB, 15KB\}$ while fixing λ at $\mu/2$ and M at 10. The results shown in Fig. 17a indicates a strong impact of the packet size on the EPD performance. For instance, the goodput ρ_g at $K = 2^8$ is equal to 0.83 for packet size 5KB, which is reduced to 0.67 for packet size 10KB and further reduced to 0.51 for packet size 20KB. The badput of the EPD is no longer negligible for large packet size even when the buffer is large. In comparison, the effect of the packet size on the PTD performance in Fig. 17b, is less significant than that on the EPD performance. In fact, the PTD performance is much less dependent on the packet size for large buffer systems.

Now we investigate the performance of PTD and EPD as a function of the number of i.i.d. sources $M \in \{5,\ 10,\ 15\}$. All the other factors are fixed at $\rho = 2$, $K = 2^{10}$, $K_0 = K/2$, $\lambda = \mu/2$, and $\lambda\beta^{-1}$ =10KB. Note that the OFF-period of each source needs to be readjusted in order to keep $\rho = 2$ unchanged at each given M. It is clear that the traffic will become burstier for larger M. The results of the PTD and EPD performance are summarized in Table 1. Again, EPD performs remarkably better than PTD for any number of sources as measured by ρ_g and ρ_b. As M increases from 5 to 15, the ρ_g of EPD only experiences a slight reduction from 1.0 to 0.96. Yet, the ρ_g of PTD has dropped from 1.0 to 0.48 just as M is changed from 5 to 10. In the overload condition, the P_g of PTD and EPD is always close to $\frac{1}{\rho}$ for large buffer size, less sensitive to M as shown in Table 1.

		P_g	ρ_g	ρ_b
$M = 5$	PTD	0.503	1.0	0.0
	EPD	0.497	1.0	0.0
$M = 10$	PTD	0.503	0.480	0.520
	EPD	0.499	0.962	0.037
$M = 15$	PTD	0.503	0.474	0.525
	EPD	0.489	0.969	0.010

Table 1: Effect of number of virtual connections on PTD and EPD performance.

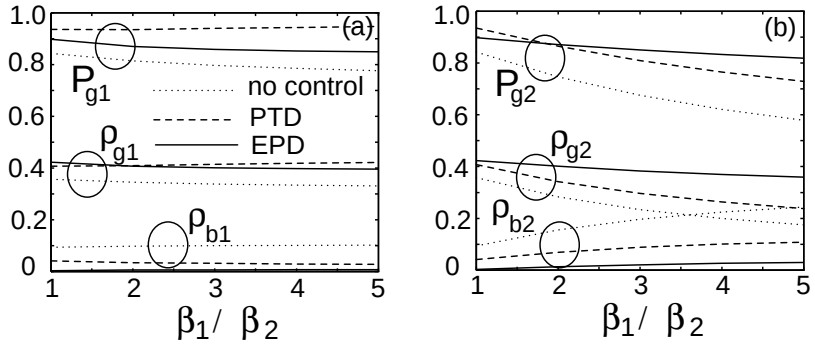

Figure 18: Effect of β_1/β_2 on (P_g, ρ_g, ρ_b): (a) source 1; (b) source 2.

5.3 Effect of Heterogeneous ON/OFF Sources

So far, we have considered homogeneous data sources only. In real ATM networks, data sources are likely heterogeneous. For the sake of analysis, here we only consider the integration of two types of heterogeneous sources, each of which is modeled by a two-state Markov chain as in the previous modeling. The same notations are used here with $(\lambda_i, \beta_i, M_i)$ for source type $i = 1, 2$. Assume four i.i.d sources of type 1 and four i.i.d. sources of type 2 in the system, i.e., $M_1 = M_2 = 4$. The performance of each type is measured by $(P_{gi}, \rho_{gi}, \rho_{bi})$. The overall performance can then be expressed by

$$\begin{aligned} P_g &= \frac{\rho_1\lambda_2\beta_2^{-1}P_{g1}+\rho_2\lambda_1\beta_1^{-1}P_{g2}}{\rho_1\lambda_2\beta_2^{-1}+\rho_2\lambda_1\beta_1^{-1}}, \\ \rho_g &= \rho_{g1} + \rho_{g2}, \\ \rho_b &= \rho_{b1} + \rho_{b2}, \end{aligned}$$

where ρ_i is the loading factor for source type i. Again, we take $K = 2^{10}$ and $K_0 = K/2$. The system is loaded by $\rho = 0.95$ with $\rho_1 = \rho_2 = \rho/2$.

Ws first study the effect of the packet size difference between the two source types. The peak cell arrival rate of the two source types are made identical and fixed at $\lambda_1 = \lambda_2 = \mu/2$. The packet size of source type 1 is set at $\lambda_1\beta_1^{-1}$ =10KB while the packet size of source type 2, $\lambda_2\beta_2^{-1}$, is adjustable. The ratio of type 2 source packet size to type 1 source packet size is then represented by β_1/β_2. Plotted in Fig. 18 are the resulting performance of individual source types for the three schemes as a function of $\frac{\beta_1}{\beta_2} \in [1,\ 5]$. As one can see, the performance of source type 1 is not significantly affected by the change of source type 2 characteristics. Comparatively, the performance of source type 2 deteriorates notably as β_2 reduces, due to the increased burstiness of type 2 traffic as discussed in Section 5.2.

We now examine the effect of peak rate ratio $\frac{\lambda_1}{\lambda_2}$ of the two source types while fixing their packet size

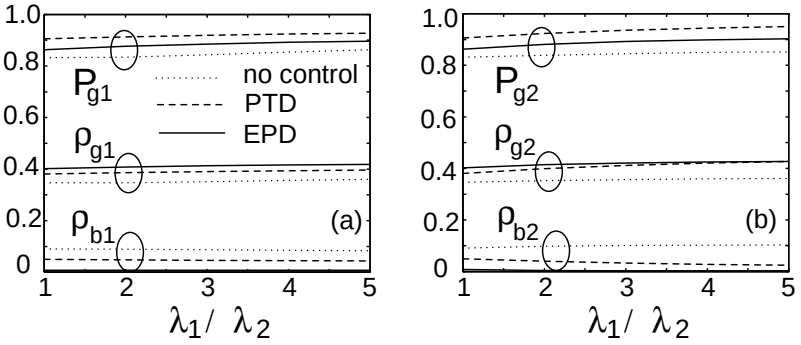

Figure 19: Effect of λ_1/λ_2 on (P_g, ρ_g, ρ_b): (a) source 1; (b) source 2.

$\lambda_1\beta_1^{-1} = \lambda_2\beta_2^{-1}$ =10KB. Take $\lambda_1 = \mu$ and adjust λ_2 in the range $[0.20\lambda_1,\ \lambda_1]$. The corresponding results are plotted in Fig. 19. The performance of both source types basically remains unchanged by $\frac{\lambda_1}{\lambda_2} \in [1,\ 5]$. This is expected since type 1 traffic is always burstier than type 2 traffic and so to a certain extent it dominates the system performance.

5.4 Effect of Window Flow Control

Our emphasis here is placed on the effect of window size, measured by $\frac{\beta}{\beta_W}$. The system is designed by $K = 2^{11}$, $K_0 = 2^{10}$, $\lambda = \mu/2$, $\lambda\beta^{-1}$ = 10KB and $M = 10$. Fig. 20(a-c) provides the solutions of the three schemes as a function of $\frac{\beta}{\beta_W} \in [1,\ 100]$ at $\rho = 0.95$. The performance drops quickly when the window size is increased from 1 to 10. Note that the last packet of each window on average is smaller than the rest of the packets due to our modeling, whereas the measure $\frac{\beta}{\beta_W}$ does not reflect such an adjustment of the last packet size. Hence, the good performance appeared in Fig. 20 with small window size is somewhat inflated by the last packet adjustment. Also note that the sources always become more persistent with increased window size, which can cause more network congestion unless with proper packet discarding schemes. This is clear especially when the window size is larger than 10 times of the average packet size. As the window size further increases, PTD and noncontrolled scheme still shows performance degradation, whereas EPD scheme maintains relatively constant performance.

Another observation is made in Fig. 20(d-f) in the overload condition characterized by $\rho = 2$. The noncontrolled and PTD schemes show some performance improvement as the window size increases from 1 to 10. The EPD scheme achieves virtually 100% goodput and 0% badput for all the window sizes. The inspection of Fig. 20(a-e) and (d-f) indicates that the performance difference in the three schemes is further broadened in the overload condition. Clearly, the performance advantage of EPD over PTD and noncontrolled becomes even more significant with the window flow control.

5.5 Effect of Underlying Traffic

So far our study has assumed the existence of data only traffic in the ATM networks. In reality, the link bandwidth is dynamically shared with other traffic, particularly with the real-time traffic which often has a high transmission priority. In most applications, data services have stringent loss rate requirement but can tolerate much time delay variations. With high-priority transmission of real time traffic, the data traffic will be served by the variable remaining link bandwidth. In the stochastic modeling, one can use a Markov chain modulated rate process to characterize the time varying behavior of the remaining link bandwidth, which directly reflects the time varying behavior of the underlying real time traffic. As found from many

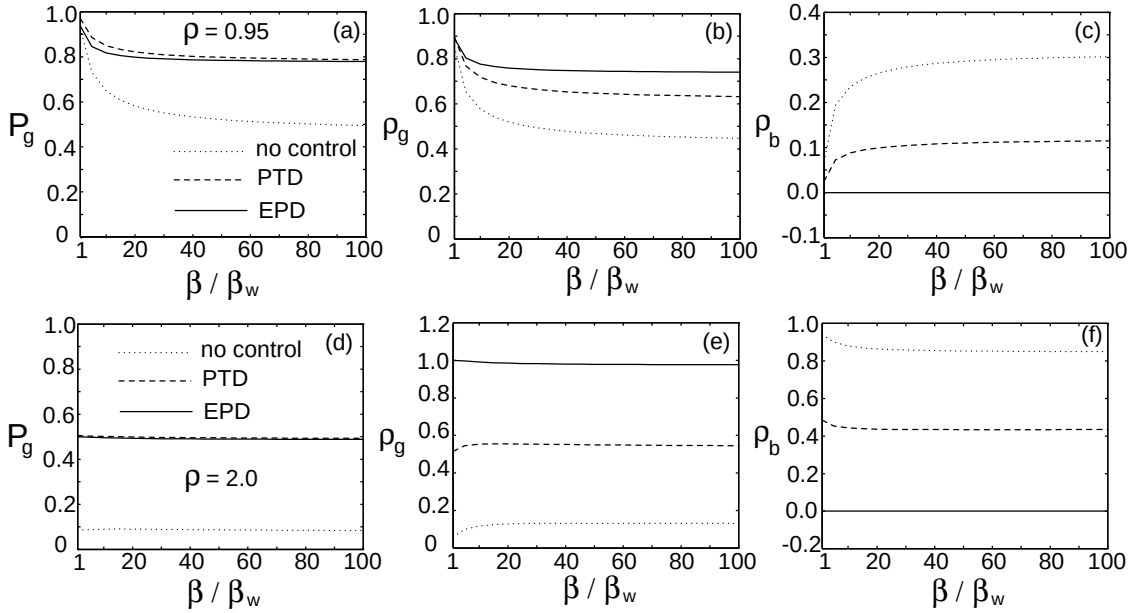

Figure 20: Effect of window size on : (a-c) (P_g, ρ_g, ρ_b) for $\rho = 0.95$; (d-f) (P_g, ρ_g, ρ_b) for $\rho = 2.0$.

measurement-based studies, most real time traffic exhibit strong correlation and burstiness nature in a wide range of time scales.

For simplicity, here we will use the superposition of four i.i.d. two-state Markov chains to modulate the data transmission rate $\mu(t)$. The autocorrelation function of $\mu(t)$ can then be expressed by $R(\tau) = \psi e^{\lambda_u \tau}$, where λ_u is the real eigenvalue of the two-state Markov chain and ψ is a weighting factor. In our case, we simply choose $\lambda_u = \lambda^\bullet / T$ at a given $\lambda^\bullet = -0.115$, such that $T \in [10^{-6},\ 1]$ is adjusted to reflect the relative timescale change of the data transmission rate. Thus, a larger T corresponds to a larger timescale of the service process and vice versa. One can also write $\psi = \overline{\mu}^2 C^2$, where C is the variation of coefficient of the data transmission rate which is set at 0.5. $\overline{\mu}$ is the average data transmission rate.

For the buffer design, we choose $K = 2^{10}$ and $K_0 = K/2$. Assume that the original link bandwidth $\mu = 155$Mbps is loaded at $\rho = 0.96$, 50% of which is taken out for the real time traffic transmission (i.e., $\overline{\mu} = 80.6 Mbps$). Each data source is described by $\lambda = \mu/2$ and $\lambda\beta^{-1}$=10KB with $M = 10$.

Plotted in Fig. 21a are the solutions of P_g, ρ_g, and ρ_b for the data transmission. We observe the data performance degradation as the timescale T of the data bandwidth increases. This is intuitively clear and consistent with other correlated queueing analyses. Also displayed in Fig. 21(b-c) is the normalized everage size of good packets and bad packets. As the timescale increases, both good and bad packet sizes for noncontrolled and PTD tend to be reduced. Yet, for EPD they are basically unchanged within the entire timescale range. This is another significant advantage of EPD over noncontrolled and PTD.

6 Conclusions

In this paper we have developed a stochastic modeling technique for packet-level performance evaluation of PTD and EPD schemes, measured by the packet success probability P_g, goodput ρ_g and badput ρ_b. We systematically studied the effect of system design parameters and source control factors on the performance of individual packet discarding schemes. We also examined the data performance with respect to the transport of heterogeneous sources, the design of window flow control mechanism and the high-priority

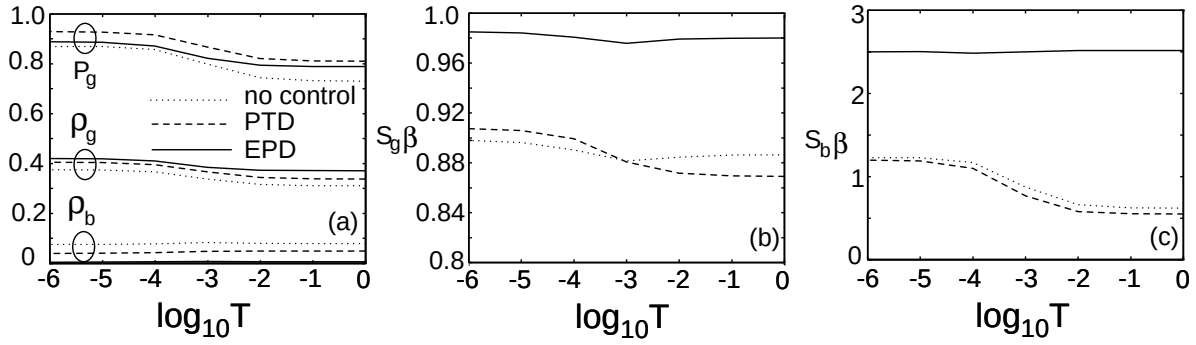

Figure 21: Effect of underlying traffic on (a)P_g, ρ_g, ρ_b; (b) good packet size; (c) bad packet size.

transmission of real time traffic. Here are some of the basic findings from our study. The system can be entirely shut down in overload period if no packet discarding control scheme is implemented. The EPD scheme always outperforms the PTD scheme significantly under most conditions, unless with sufficiently large buffer capacity. Especially under overload condition, EPD can always achieve about 100% goodput and 0% badput whereas the performance of PTD deteriorates rapidly. Among all the factors, the packet size has dominant impact on EPD performance. In the design of EPD, there is an optimal selection of the queue control threshold to achieve the maximum goodput. Finally, out modeling technique can be directly applied to the analysis of other packet discarding schemes such as the random early packet discarding proposed in [4] and the tail packet discarding with queue control threshold.

References

[1] V. Jacobson, "Congestion Avoidance and Control," *Proc. of ACM SIGCOMM'88*, Stanford, Ca., Aug. 1988, pp. 14-329.

[2] G. Armitage and K. Adams, "Packet Reassembly During Cell Loss," *IEEE Network Magazine*, Vol. 7, No. 5, Sept. 1993, pp. 26-34.

[3] S. Floyd and A. Romanov, "Dynamics of TCP Traffic over ATM Networks," *IEEE JSAC*, Vol. 13, No. 4, May 1995, pp. 633-641.

[4] S. Floyd and V. Jacobson, "Random Early Detection Gateways for Congestion Avoidance," *IEEE/ACM Trans. on Networking*, Vol. 1, No. 4, Aug. 1993, pp. 397-413.

[5] J. S. Turner, "Maintaining High Throughput During Overload in ATM Switches," *Proc. IEEE Infocom'96*, March 1996, pp. 287-295.

[6] A. E. Kamal, "Performance Modeling of Partial Packet Discarding Using the End-of-Packet Indicator in AAL Type 5," *IEEE/ACM Trans. on Networking*, Vol. 4, No. 6, Dec. 1996, pp. 929-940.

[7] A. Bhargava and M. G. Hluchyj, "Frame Losses Due to Buffer Overflows in Fast Packet Networks," *Proc. IEEE Infocom'90*, June 1990, pp. 132-139.

[8] S. Q. Li and H. D. Sheng, "Generalized Folding Algorithm for Sojourn Time Analysis of Finite QBD Processes and its Queueing Applications," *Commu. Statist.−Stochastic Models*, Vol. 12, No. 3, 1996, pp. 507-522.

[9] J. Ye and S. Q. Li, "Folding Algorithm: A Computational Method for Finite QBD Processes with Level-Dependent Transitions," *IEEE Trans. Commu.*, Vol. 42, No. 2, Feb. 1994, pp. 625-639.

[10] J. G. Kemeny and J. L. Snell, *Finite Markov Chains*, Springer-Verlag, New York, 1976.

[11] S. Q. Li and C. L. Hwang, "Queue Response to Input Correlation Functions: Continuous Spectral Analysis," *IEEE/ACM Trans. Networking*, Vol. 1, No. 6, Dec. 1993, pp. 678-692.